Coulomb-gap magnetotransport in granular and porous carbon structures

A. W. P. Fung
Department of Electrical Engineering and Computer Science, Massachusetts Institute of Technology, Cambridge, Massachusetts 02139

Z. H. Wang
Department of Physics and Francis Bitter National Magnet Laboratory, Massachusetts Institute of Technology, Cambridge, Massachusetts 02139

M. S. Dresselhaus
Department of Electrical Engineering and Computer Science and Department of Physics, Massachusetts Institute of Technology, Cambridge, Massachusetts 02139

G. Dresselhaus
Francis Bitter National Magnet Laboratory, Massachusetts Institute of Technology, Cambridge, Massachusetts 02139

R. W. Pekala
Chemistry and Materials Science Department, Lawrence Livermore National Laboratory, Livermore, California 94550

M. Endo
Shinshu University, Faculty of Engineering and Cooperative Research Center, Nagano, Japan
(Received 21 January 1994)

The possibility of observing a Coulomb gap due to carrier-carrier interactions in granular metallic systems is investigated, with particular emphasis on porous carbon structures such as carbon aerogels and activated carbon fibers (ACF's), both of which contain ultrafine pores and grains, the size of which can be controlled by the sample preparation procedures. The $\exp[-(T_0/T)^{1/2}]$ temperature dependence observed at low temperature in the dc electrical conductivity of both materials is characteristic of granular metallic systems. A variable-range hopping mechanism near a Coulomb gap around the Fermi level is proposed to circumvent the difficulties of previous tunneling and hopping models. The temperature dependence of the magnetoresistance in fields up to 15 T is measured for both aerogels and ACF's to further confirm the effect of the Coulomb gap. The results not only qualify porous materials as a medium for studying localization phenomena, but also shed some light on the complex problem of transport near the percolation threshold in granular metallic systems in general.

I. INTRODUCTION

Since the comprehensive study of granular metals (GM's) by Abeles *et al.*,[1] the question of whether variable-range hopping (VRH) or tunneling between nearest neighbors (N-N) is responsible for the transport behavior of subpercolating GM systems remains an open issue. GM's typically exhibit a temperature-dependent dc electrical resistivity $[\rho(T)]$ of the form

$$\rho(T) = \rho_0 \exp\left[\left(\frac{T_0}{T}\right)^{1/p}\right], \qquad (1)$$

where $p = 2$, ρ_0 is some proportionality constant, and T_0 varies between 10^2 K and 10^4 K depending on the metallic volume fraction (x) in the system. The same $\rho(T)$ behavior is observed in our transport results for both carbon aerogels[2] and activated carbon fibers (ACF's),[3,4] thus prompting this study of the relationship between the general localization phenomena and the granular nature of porous materials.

Earlier attempts to provide an explanation for observing Eq. (1) with $p = 2$ in GM systems have been criticized for their limitations and unrealistic assumptions.[5,6] While the critical percolation method (CPM)[7–9] gives a likely explanation for the $p = 2$ behavior for GM systems in which the granular size d is on the same order as the granular separation s, our porous systems, in which the conductive particles are necessarily nonuniformly distributed in space in order to hold the sample together even without a solid-phase insulating matrix, consist of close-packed regions with $d \gg s$ and require a new model. Our new model takes into account the effective potential barriers presented by the intervening grains, which are essential for the VRH to be operative, thus complementing the CPM studies.

Porous carbon materials can be exploited in both industrial applications and academic studies. Since the advent of the synthesis of quantum structures [e.g., quantum dots, single-electron transistors (Coulomb islands[10])], new transport phenomena have been observed and detailed studies of the transport properties

of nanosize structures have become subjects of particular interest. The recent interest in mesoscopic systems consisting of clusters of atoms in the 1–100 nm size and possessing physical properties between the molecular and the bulk solid-state limit[11] also adds appeal to the study of nanoporous materials like carbon aerogels. Previous studies of carbon aerogels show that their unique optical, thermal, acoustic, mechanical, and electrical properties are indeed very closely related to their nanostructure,[12] validating studies of porous carbon materials in their own right, not merely in the context of either quantum structures or GM systems. Finally, the development of new characterization tools for porous materials in general is beneficial to several industries, such as the optoelectronics industry where porous silicon is exploited.

We discuss in this work why VRH becomes more likely than tunneling in GM systems with $d \gg s$. In particular, both our $\rho(T)$ and the magnetoresistance (MR) results, when correlated with the previous structural characterization measurements, indicate that VRH in a Coulomb gap[13] plays a more dominant role in porous materials than tunneling, thus ruling out the fluctuation-induced tunneling model.[14] Not only does the Coulomb gap VRH model provide information about the effective dielectric constant and the grain size (given the effective mass of the charge carriers), but it also has potential applicability to GM systems near the metal-insulator transition and other porous materials.

In the following, the nanostructures of carbon aerogels and ACF's are briefly described. Following the discussion of the shortcomings and the limitations of previous transport models relevant to GM systems, the Coulomb gap VRH model is rederived for systems with finite-size particles, in a formalism that encompasses previous models in their limiting regimes. The present model is then applied to explain the different T_0 values as well as the temperature and field dependences of the magnetoresistance in carbon aerogels, ACF's, and other GM systems.

II. NANOSTRUCTURES OF CARBON AEROGELS AND ACTIVATED CARBON FIBERS

The microstructures of both carbon aerogels and activated carbon fibers (ACF's) consist of *nanoparticles* and *nanopores* (so named because they are of nanometer size) and are therefore sometimes termed nanostructures. The nanoparticles in these porous carbons are found to be rather graphitic by Raman scattering.[3,12] In carbon aerogels, these nanoparticles further cluster to form larger *particles*. The admixtures of the conductive grains, namely, the nanoparticles in ACF's and the particles in carbon aerogels, and the insulating pores hence constitute a new class of GM systems, possibly complementary to those found in Cermets[1] and discontinuous thin films,[6] because of the different spatial distributions of the grains in these materials. The different morphologies of carbon aerogels as compared to ACF's further allow the study of two strongly localized systems with totally different structural characteristics (e.g., granular size, grain separation, distribution, interconnection, and dimensionality). Within each class of materials, further fine tuning of the nanostructural parameters is possible, as described below.

Carbon aerogels possess the morphology as illustrated in Fig. 1 and have a very low mass density ($\rho_m = 0.1$–0.6 g/cm^3). Five different features can be identified in typical transmission electron microscope (TEM) micrographs for aerogels, on which Fig. 1 is based.[15] Of relevance to us are the beadlike particles (feature c) and the neck region between neighboring particles (feature e). The samples used in this work have a particle size $\sim 12 \pm 1.5$ nm in diameter. High-resolution TEM (not shown) reveals the glassy-carbon-like nanostructure in the particle and the neck regions,[16] both of which are composed of nanoparticles and nanopores. This nanostructure is supported by the Raman scattering measurements,[12] from which the in-plane microcrystallite size ($L_a \sim 2.5$ nm) is known to be smaller than the particle size. The skeletal density of 2.06 ± 0.06 g/cm^3 found by helium pycnometry[15] for carbon aerogels synthesized at a [resorcinol]/[catalyst] (R/C) ratio = 200 also suggests that these glassy carbon ribbons (nanoparticles) are probably relatively graphitic, since the density of typical glassy carbons is 1.46–1.50 g/cm^3, whereas that of graphite is 2.26 g/cm^3. With frequent contacts among the glassy carbon ribbons which are entangled with each other within the particle, the particle can be thought of as the conductive grain in this GM system. The nanopores in the neck region between particles thus

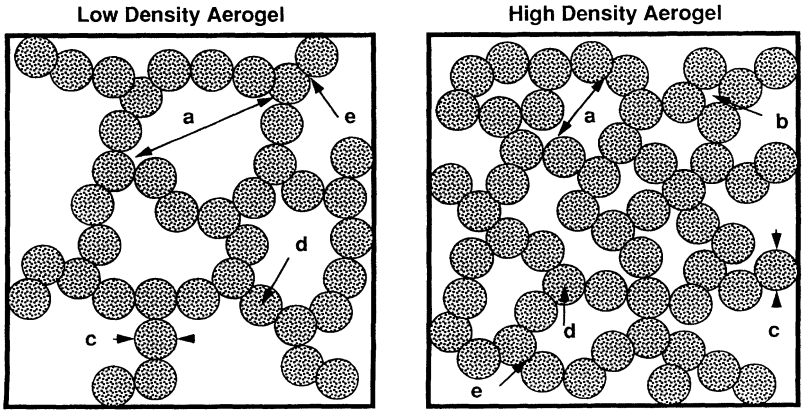

FIG. 1. Schematic diagram showing the following features of the carbon aerogel microstructure and nanostructure as a function of bulk density: *a*, mesopore that spans the distance between chains of interconnected particles; *b*, micropore sandwiched between particles; *c*, individual particle ($\sim$ 12 nm diameter); *d*, micropore showing nanostructure within the particles, and *e*, neck region between contiguous particles.

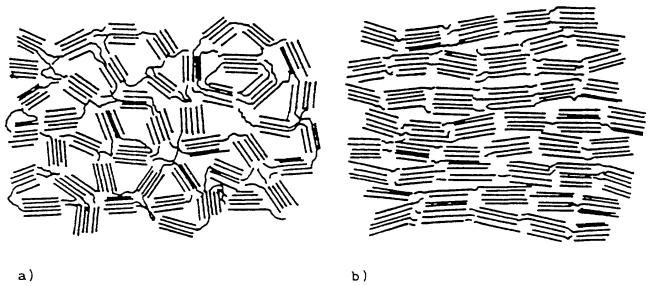

FIG. 2. A schematic diagram showing the difference between the nanostructures of (a) as-prepared ACF's and (b) heat-treated ACF's with $T_{HT} = 850\,^{\circ}C$. The thickness of the microcrystallites shown in the figure is only approximate. The microcrystallites in ACF's should really be 1–3 layers thick. (Figures based on the model from Ref. 43.)

provide an upper limit for the tunneling distance between two conducting grains.

While the R/C ratio can be used to control the particle size in carbon aerogels, the mass density determines the packing ratio or interconnectivity. With increasing mass density, the particle size remains constant but the packing ratio of these particles increases. In this study, the R/C ratio is fixed at 200 and the mass density is varied so that a density dependence of the transport properties can be studied.

In as-prepared ACF's,[3] the conducting grains are the nanoparticles, which are graphite platelets 1–3 layers thick and ~2.5 nm in diameter. ACF's are also a unique class of porous materials in which the total porous volume is almost entirely made up of micropores, whose average size is on the order of 1 nm. Hence, the specific surface area (SSA) (up to $3000\,m^2/g$) and the mean number of nanopores per unit volume of as-prepared ACF's is much larger than in carbon aerogels. However, the mass density of ACF's ($\sim 1.6\ g/cm^3$) is much higher because of the low density of mesopores, which are typically larger than 2 nm in size, and the large packing ratio of graphite platelets, as depicted in Fig. 2. Locally, some neighboring platelets that are separated on an atomic scale are more or less aligned in short sections in the in-plane direction but globally, the platelet-to-platelet angles are randomly and widely distributed. The micropores are accordingly bounded by the c faces of the graphite platelets and their narrowest dimension is measured to be ~ 10 Å.

Heat treatment at temperatures below 1000 °C causes the platelets in ACF's to align without registry along the c axis, but such heat treatment does not change the in-plane size of the platelets significantly.[17,18]

III. EXPERIMENTAL DETAILS

The preparation and characterization of carbon aerogels have been described elsewhere.[12] The carbon aerogels in this study were all synthesized at the same R/C ratio of 200 and pyrolyzed at 1050 °C, a temperature value within the range of that typical for disordered carbons to undergo a metal-insulator transition (1000–1200 °C for ACF's[4]). The density was controlled (from $\rho_m \sim 0.1$ to $\sim 0.65\ g/cm^3$) by varying the reactant concentrations of the starting solution.

The manufacturing procedure for the synthesis of the as-prepared phenol-based ACF's (supplied by Kuraray Chemical Co. in Japan) is described in Refs. 3, 19, and 20. The phenol precursors are activated at temperatures between 800 and 1100 °C in O_2, H_2O, CO_2, or other oxidizing atmospheres. The activation process results in a specific surface area (SSA) in the range 1000–2000 m^2/g. Prior to heat treatment, the phenol-based ACF's used in this study have a SSA of 1000 m^2/g. These ACF's are subsequently heat treated at 850 °C in an argon atmosphere for about 1 h. The length of the fiber sample is measured by an optical microscope (~1 cm) and the diameter by a scanning electron microscope ($\sim 10\,\mu m$). The structural characterization of these fibers is described elsewhere.[3,17,18]

All dc electrical transport measurements were made by the four-probe method. Electrical contacts with the fiber and the aerogel samples are made with silver paint and silver epoxy, respectively. The latter is selected because of its high viscosity and its good adhesion to the aerogel surface. Current leads to the aerogel samples were made at both ends of the samples which measure $\sim 8 \times 3 \times 3\ mm^3$. Since carbon aerogels of low mass density are poor thermal conductors, the temperature homogeneity within the sample, and the temperature equilibrium between the sample and the environment, were ensured by allowing all temperature scans to take place by natural warming (e.g., 2 h from 1.5 K to 4.2 K). All magnetoresistance measurements (in a field up to 15 T) were made only after the resistances of the samples had reached their steady state values. The magnetoresistance was measured with a superconducting magnet in the Francis Bitter National Magnet Laboratory at MIT.

IV. EXPERIMENTAL RESULTS

The temperature-dependent electrical conductivity and magnetoresistance for both ACF's and carbon aerogels are presented in this section. Results from other relevant characterization measurements are used to interpret these transport results.

Measurements of the resistivity ρ in as-prepared and heat-treated ($T_{HT} = 850\,^{\circ}C$) ACF's were carried out from 4.2 K to 300 K. The many-decade change of ρ in the same ACF's at low temperature ($T < 100$ K), as shown in the ρ versus T plots in the inset to Fig. 3, is characteristic of a strongly localized system. It is remarkable that the strongly temperature-dependent ρ over the temperature range 4 K $< T <$ 100 K for both the as-prepared and the heat-treated ACF's were well fitted by Eq. (1) for $p = 2$ and with $T_0 = 530$ K and 92 K, respectively, as shown by the solid lines in Fig. 3, where the data points for $\log_{10}\rho$ are also plotted versus $1/T^{1/2}$. In both the inset and the figure in Fig. 3, the temperature dependence of $\rho(T)$ is weaker and the absolute magnitude of ρ is lower in the heat-treated ACF than in the as-prepared

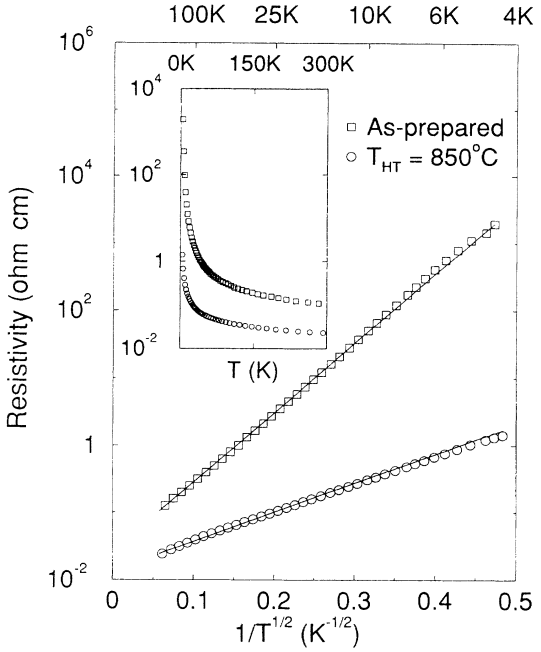

FIG. 3. Logarithmic resistivity versus $1/T^{1/2}$ for both the as-prepared and the ACF's heat-treated at 850 °C, with specific surface area (SSA) = 1000 m^2/g for both samples. The x axis on top of the figure gives the temperature directly. The inset plots the same logarithmic resistivity curves as a function of linear temperature to show the drastic change in resistivity at low temperature.

ACF because heat treatment brings ACF's closer to the metal-insulator (MI) transition conditions.

Raman scattering measurements[18,21] show that the in-plane microcrystallite size does not increase by much upon heat treatment at T_{HT} = 850 °C. Thus, fusion between neighboring platelets has not yet taken place and the granular size can be assumed to remain at ~ 30 Å, the same value observed in the as-prepared ACF's.[3] Brunauer-Emmett-Teller (BET) measurements[18] indicate, however, that the collapse of micropores begins when T_{HT} reaches ~ 1000 °C. It is conceivable that the graphite platelets have at least begun to realign preferentially along the c axis, consequently forming an easier path for conduction than in the as-prepared ACF's. Nevertheless, metallic conductivity is still not achievable in these heat-treated ACF's, as indicated by the zero value of the conductivity $\sigma(T = 0)$ at zero temperature and the negative temperature coefficient of resistivity (TCR). This is because the narrow necks (constrictions) connecting the neighboring platelets (approximately a single-bond length apart) *are not necessarily electrically conductive*, although coupled platelets are needed to hold the porous sample together. The short distance of this somewhat insulating spatial gap is essential for the applicability of the variable-range hopping mechanism discussed later.

The $p = 2$ behavior observed in both ACF's in Fig. 3 implies universality in the transport properties of all ACF's, which now constitute one class of GM systems, and suggests the use of the heat-treated ACF's, which have a lower resistance at low temperature, in a representative magnetoresistance (MR) study of ACF's. The MR measurements for the as-prepared ACF are omitted in the present paper because the effect of heat treatment on the transport properties, including the low-field MR of ACF's, has been studied elsewhere[4] and is not the subject of this work. Upon progressive heat treatment, but still below the MI transition, the positive MR of the heat-treated ACF's gradually decreases in magnitude.[4]

The MR curves for the ACF heat treated at 850 °C at different measurement temperatures are plotted in Fig. 4 on different vertical scales to illustrate the approximately parabolic field dependence at low field. The anomalous MR curve at 50 K (higher than that at 30 K) might have been due to the ineffectiveness of the capacitance temperature sensor in holding the temperature steady in a high field at this temperature. All MR curves follow a quadratic field dependence at low field. While the magnitude of the MR increases with decreasing temperature, the field value for the onset of deviations from the quadratic field dependence decreases at the lowest measurement temperatures (< 7 K).

Positive MR in a VRH system can be explained by the field-induced shrinkage of the wave function.[22] Accompanying the reduced wave-function overlap is a decrease in the probability of tunneling and hence an increase in the resistance. The temperature and the field dependence of the positive MR in the low-field limit are given by[22]

$$\ln\left[\frac{\rho(H)}{\rho(0)}\right] = t\left(\frac{\xi}{\lambda}\right)^4\left(\frac{T_0}{T}\right)^{3/p} \equiv AH^2 , \qquad (2)$$

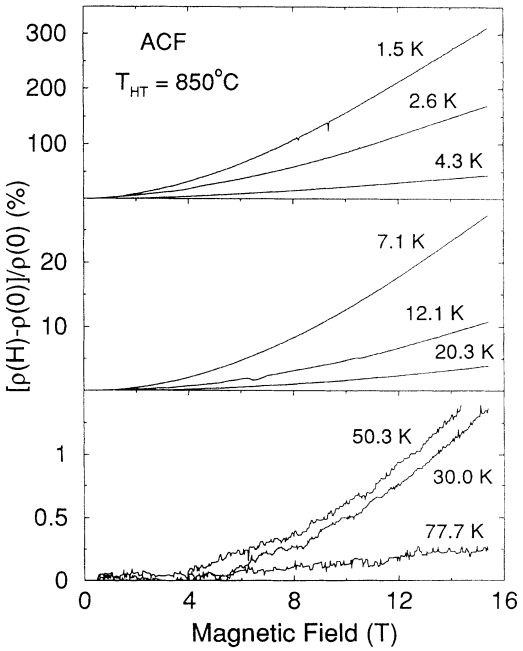

FIG. 4. Transverse magnetoresistance for the ACF's heat treated at 850 °C at the indicated measurement temperatures. The y axis is divided for clarity into three different scales according to the relative magnitudes of the data.

where $\lambda = \sqrt{\hbar c/eH}$ is the magnetic length, ξ is the localization length of the wave function, p is the same exponent as in Eq. (1), and t, typically on the order of 0.001, is p dependent. From fitting the $\ln[\rho(H)/\rho(0)]$ data at low field versus H^2, the quadratic coefficients A as defined in Eq. (2) are obtained as a function of temperature. As plotted in Fig. 5, the slope of $\log_{10} A$ versus $\log_{10} T$ obtained from a linear fit is $\simeq 1.8 \pm 0.2$, implying that $p \sim 2$ if $A \propto 1/T^{3/p}$.

In Fig. 6, the logarithmic resistivities are plotted against $1/T^{1/2}$ for carbon aerogels of different densities. Except for the low-density (LD) sample which exhibits a seven-decade increase in the resistivity from 10 K down to 2 K, the temperature dependence of the resistivity for both the intermediate-density (MD) and the high-density (HD) samples is relatively weak, changing by less than two decades over the entire measurement temperature range 1.5 K $< T <$ 300 K. Indeed, the high packing ratio of the grains in the MD and the HD samples resembles the situation in the heat-treated ACF discussed above, or, in general, in any GM system close to the MI transition.

All samples in Fig. 6 show the $p = 2$ behavior in Eq. (1) at very low temperature ($<$ 10 K) with $T_0 = 2100$, 200, and 30 K for the LD, MD, and HD aerogel samples, respectively. As discussed later, the large dielectric constant near the MI transition narrows the spread of the charging energy of the grains. Being a measure of this energy spread, T_0 should decrease with increasing density. At higher temperatures, deviations from linearity of $\log_{10} \rho$ with $1/T^{1/2}$ are observed for the LD and MD samples for complicated reasons given later.

The MR data for the 0.457 g/cm^3 (MD) carbon aerogel sample are plotted in Fig. 7 as a function of magnetic field for various temperatures. Similar MR curves (not shown) with lesser magnitude for the quadratic field dependence at a given temperature are observed for aerogel samples with higher densities and were published elsewhere.[12]

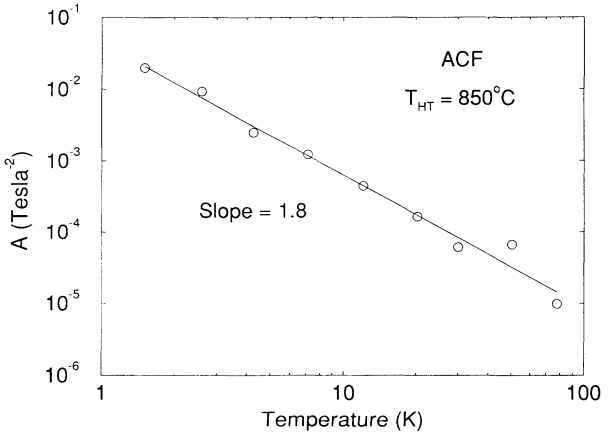

FIG. 5. Log-log plot of the quadratic coefficients A (see definition in text) extracted from the low-field transverse magnetoresistance measured for the ACF heat treated at 850 °C. Each data point is for magnetoresistance measurements made at the indicated measurement temperature. The solid line is a linear fit to the log-log plot which shows a slope of ~ 1.8.

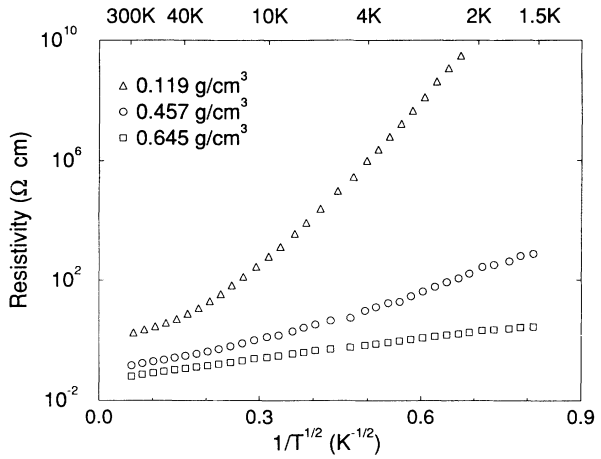

FIG. 6. Logarithmic resistivity versus $1/T^{1/2}$ for carbon aerogels of labeled densities. The upper scale gives the actual measurement temperatures.

We made two series of measurements with each sample to eliminate the artifacts in the MR measurements due to temperature inhomogeneity and nonequilibrium. For graphical clarity, only the second set of quadratic coefficients A, which are close to the A values obtained from the first run, are plotted in Fig. 8. The slopes for the $\log_{10} A$ versus $\log_{10} T$ curves in Fig. 8 all read approximately 1.5 ± 0.3 below 10 K, corresponding to $p \sim 2$, again consistent with the $\sigma(T)$ behavior at low temperature.

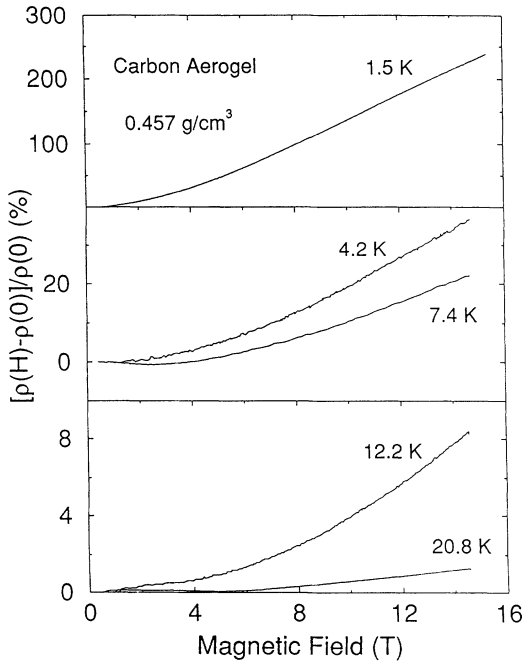

FIG. 7. Transverse magnetoresistance for a carbon aerogel sample with a mass density of 0.457 g/cm^3 at various temperatures.

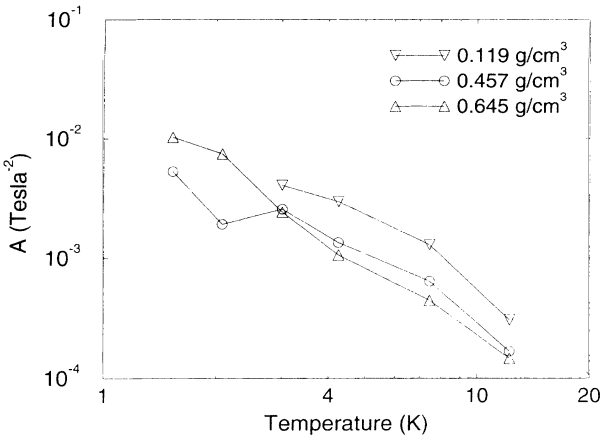

FIG. 8. Log-log plot of the quadratic coefficients A (see text) extracted from the temperature-dependent magnetoresistance data obtained for carbon aerogels of three different mass densities in the second run. Below 10 K, the slopes of all the $\log_{10} A$ versus $\log_{10} T$ curves are ~ 1.5.

V. DISCUSSION OF TRANSPORT MODELS

The limitations and shortcomings of previous transport models are discussed in connection with porous materials in this section.

The first attempt to explain the $p = 2$ conductivity behavior of Eq. (1) was the model of Ref. 1, which utilizes the concept of a charging energy $E_c \sim e^2/\kappa d$ that is required to put a charge e through a medium with dielectric constant κ onto a neutral grain of diameter d. This single-junction tunneling model and a later numerical study[23] using the critical path method (CPM) both suffer from their two underlying assumptions, namely, that the grain separation s and diameter d are locally correlated, and that both are widely distributed, both of which are unsubstantiated by the experimental observations in most GM systems,[7,24] including our porous carbon systems.

The most promising nearest-neighbor (N-N) hopping model so far is provided by the numerical and theoretical studies using the critical path method with independent sets of uncorrelated distributions for s and d, which are on the same order.[7–9] It was found theoretically[8,9] that VRH exists in GM systems only at very low temperature and that the $p = 2$ behavior is merely an interpolation between VRH over multiple grains at low temperature and N-N grain-to-grain hopping at high temperature. In porous carbons, however, $d \gg s$ and the hopping distance, given by $R \sim (\hbar/\sqrt{2m\phi})(T_0/T)^{1/p} d/(s+d)$, where ϕ is the tunneling barrier, could exceed the N-N center-to-center distance $s+d$, implying the possibility of VRH.

The one-dimensional (1D) VRH model is one VRH model with $p = 2$ but neither the glassy-carbon structure within a grain in carbon aerogels nor the beadlike granular configuration can be a medium for 1D VRH. Regarding the glassy-carbon structure, transport is dominated by free carriers, not localized carriers, because the photoconductivity ($\Delta\sigma_{\rm ph}$) results for both the ACF's (Ref. 25) and the carbon aerogels[26] show that $\Delta\sigma_{\rm ph}/\sigma < 1$ even at low temperature and hence that the dark carrier concentration, being larger than the photocarrier concentration, is not small. Although localization is in the present case achieved with a grain boundary, quasi-1D structures composed of these grains are still lacking because of the high packing ratio and hence high coordination number of grains in ACF's and high-density carbon aerogels. The high packing ratio should also preclude the possibility of any high-resistance blockade predicted by the quasi-1D localization transport model proposed by Brenig *et al.*[27] for a bundle of parallel and uncoupled 1D chains of finite length. Indeed, the temperature-dependent transport properties in both the ACF's and the carbon aerogels with different mass densities are very similar despite the difference in their chain lengths L.

Another VRH model with $p = 2$ is proposed in connection with the Miller-Abrahams network[28] which models the conductivity σ between any pair of nodes (e.g., i and j), separated by r_{ij} in distance and ϵ_{ij} in energy, according to

$$\sigma = \sigma_0 \exp\left(-\frac{2r_{ij}}{\xi} - \frac{\epsilon_{ij}}{k_B T}\right) , \tag{3}$$

where σ_0 is some conductivity constant and ξ the localization length. If carrier-carrier (excitonic) interaction is included,

$$\epsilon_{ij} = \begin{cases} |\epsilon_j - \epsilon_i| - \frac{e^2}{\kappa r_{ij}} , & (\epsilon_i - E_F)(\epsilon_j - E_F) < 0 , \\ \max\{\, |\epsilon_i - E_F| , |\epsilon_j - E_F| \,\} , & \\ \qquad (\epsilon_i - E_F)(\epsilon_j - E_F) > 0 , & \end{cases} \tag{4}$$

resulting in a stability condition

$$|\epsilon_j - \epsilon_i| - \frac{e^2}{\kappa r_{ij}} \geq 0 \tag{5}$$

because neutral grains abound in a low-energy system. Efros and Shklovskii (ES)[13] showed that the above inequality [Eq. (5)] causes a Coulomb gap to develop near E_F and that the resistivity $\rho(T)$ should follow Eq. (1) with $p = 2$ and

$$T_0 = \frac{\beta e^2}{k_B \kappa \xi} , \tag{6}$$

where β is a dimensionless factor on the order of unity.

The Coulomb gap variable-range hopping (CGVRH) expression has also been shown to fail to apply to GM systems,[6] with the mere substitution[6,29] of the effective decay length $s/\chi(s+d)$ [see Eq. (7)] for ξ, because the hopping distance $R \sim \xi\sqrt{T_0/T}$ was shown not to convincingly exceed the N-N distance $s+d$ when $s \sim d$, without yielding an unrealistically small insulating gap barrier. Yet, both conditions can be satisfied in porous carbons or possibly GM systems near the metal-insulator (MI) transition, where $d \gg s$, as discussed below.

VI. COULOMB GAP VARIABLE-RANGE HOPPING

In this section, we describe the CGVRH model and show that the model is not affected by the finite size of the grains at low temperature.

Hopping beyond the N-N sites dictates that Eq. (6) be extended to include the wave-function decay within the hopping distance r_{ij}. The decay occurs over both the intervening gaps with average barrier height ϕ_s and width s, and the intervening grains with average barrier height ϕ_d (see below) and width d. Noting that the total distances over the intervening gaps and over the grains are on the average given by $rs/(s+d)$ and $(r-s)d/(s+d)$, respectively, we replace the Wentzel-Kramers-Brillouin (WKB) reciprocal decay length by its average,

$$\chi_{\text{eff}} = \chi_s \frac{s}{s+d} + \chi_d \frac{d}{s+d} , \tag{7}$$

where $\chi_i = \sqrt{2m_i\phi_i/\hbar^2}$ with the subscript i denoting either s or d depending on the region of relevance. With $\exp[-2\chi_d sd/(s+d)]$ absorbed into the prefactor σ_0 and the substitution of χ_{eff} for $1/\xi$, Eq. (3) now describes a Miller-Abrahams network of finite-size localization sites.

We now discuss and estimate the effective barrier presented by a grain, i.e., ϕ_d. When the wave-function decay in a metallic grain is negligible, then N-N hopping should be more likely than VRH to be the transport mechanism, as pointed out in Ref. 11. Fluctuations in the granular energy, however, make VRH possible by providing a scenario in which a N-N hop is not as energetically favorable as a distant hop. Fluctuations also provide a means of carrier localization in the form of an effective barrier in the case that the gap barrier is small ($\chi_s s < 1$), such as in porous carbon materials. In porous materials, it is necessary that the grains be linked structurally (but not necessarily electrically) in order to hold the sample together. These links as well as the image force between the N-N grains could significantly narrow s and lower ϕ_s so that $\chi_s s \ll \chi_d d$ and only the wave-function decay in the intervening grains due to granular energy fluctuations becomes important. The difficulty previously encountered when applying the original CGVRH model, namely, that a large hopping distance and a large hopping barrier are inconsistent with each other, can now be circumvented because ϕ_d is typically much smaller than the work function of metals, and the hopping distance $R \sim \chi_d^{-1}\sqrt{T_0/T}$ can be quite long relative to d provided that the χ_d associated with ϕ_d is small.

There are two kinds of fluctuations in the granular energy. Adkins[5] postulated that in a disordered system like a GM, there exists a random disorder potential in the surroundings of each grain, changing the charging energy E_c of that grain by an amount not exceeding its original charging energy, since a discharge to the ground state would result for a larger change in E_c. Consequently, given a sharp distribution for the granular size as in carbon aerogels, the perturbed energy of the system is then uniformly distributed within the range $E_F \pm 2E_c$. The second kind of energy fluctuation arises from the quantum size effects of the grains, which cause an energy level splitting within an individual grain on the order of E_F/N, where $N \propto d^3$ is the number of carriers present on the grain.[30,31] In carbon aerogels, $d \sim 120$ Å, $E_c \sim 120/\sqrt{\kappa}$ meV, $E_F \sim 1$ meV, and the free-carrier concentration is $n \sim 10^{19}$ cm^{-3} [typical of disordered carbons and also supported by superconducting quantum interference device (SQUID) measurements[12]]. Therefore, we conclude that $E_c \gg E_F/N$ in porous carbons. The same condition applies in GM's well below the percolation threshold.[1]

The effective barrier ϕ_d should be on the order of the fluctuation of the charging energy. Hence, on averaging over the energy width of $E_F \pm 2E_c$,

$$\phi_d \simeq 2E_c = \frac{2e^2}{\kappa d} . \tag{8}$$

The full algebraic details leading to a rigorous percolation solution to the Miller-Abrahams network associated with a GM or porous system involving the excitonic interaction can be found in analogy with the approximate solution by ES (Refs. 22 and 32) for the point-size site percolation problem and will only be outlined below. We use for GM systems the same density of states (DOS) derived[33,34] for point-size localization sites because the low DOS inside the Coulomb gap implies a large effective grain-to-grain separation which renders the finite size of the grains irrelevant.

In the doped semiconductor case, the critical volume fraction for quantum percolation (Θ_c) is assumed to be temperature invariant, so that the high-temperature Θ_c value can be used to solve the full VRH equation at low temperature. It is well documented[22,32] that $\Theta_c = 0.23$ for impurity conduction in semiconductors in the high-temperature regime, where N-N hopping dominates. It is tempting to follow the same procedure for GM systems with finite-size particles by using the Monte Carlo results obtained by Scher and Zallen (SZ)[35] for the site percolation problem in lattices morphologically similar to our porous carbon materials. However, we note that Θ_c is in fact *not* temperature invariant in GM systems, in which the low-temperature Θ_c value is changed to 0.15 due to the finite size of the grains.[35] Further noting that the long hopping distance implied by VRH could readily nullify the finite-size effect, we propose that $\Theta_c = 0.23$ for both GM's and doped semiconductors at low temperature, and that Θ_c remains temperature invariant in GM systems at least throughout the VRH regime. Equation (1) is therefore obtained with $p = 2$ and $\beta = 2.6$ for 3D, which agrees with the empirical value of $\beta = 2.8$ from a numerical simulation.[32] Since no empirical or theoretical value for β in 2D is available, we use the same approximate, yet reliable, procedure with the 2D DOS to obtain $p = 2$ and $\beta = 6.2$ for 2D CGVRH.

In analogy with the Green's function formalism used by ES,[22] the derivation for the magnetoresistance (MR) in the CGVRH model can be reproduced for the GM case by replacing the Coulomb potential with a step potential and substituting $1/\chi_{\text{eff}}$ for ξ. The resultant magnetic energy term $(r_{ij}^3/18\lambda^4\chi_{\text{eff}}$ in 3D and $r_{ij}^3/24\lambda^4\chi_{\text{eff}}$ in 2D, where r_{ij} is the distance between the two grains involved in a hop) is then added to the exponent in Eq. (3). Un-

TABLE I. Various physical parameters for granular or porous materials including the metallic volume fraction (x), the granular size (d) and separation distance (s), the experimental value of T_0, the dielectric constant measured (or assumed) in the insulator (κ_{ins}), calculated by the effective medium theory [κ(EMT)] and extracted from T_0 (K), the conduction mechanism involved, and its associated effective decay length χ_{eff}^{-1}, and finally the effective mass (m/m_0).

Materials	Cermet	Granular	Carbon aerogel			ACF	
		Al film	$\sim 0.119\,g/cm^3$	$\sim 0.457\,g/cm^3$	$\sim 0.645\,g/cm^3$	as-prepared	850 °C
x	0.24	0.5	0.058	0.222	0.313	–	–
d (Å)	24[a]	30	120	120	120	30	> 30
s (Å)	11[a]	2	2	2	2	2	2
T_0 (K) (expt)	16000	200	2100	200	30	530	92
Conduction mechanism	NNH	CGVRH	CGVRH/NNH[b]	CGVRH/NNH[b]	CGVRH	CGVRH	CGVRH
κ_{ins}	4	8	2	2	2	2	2
κ (EMT)	14	80	2	6	33	–	–
κ (expt)	–	110	6	31	110	27	110
χ_{eff}^{-1} (Å)	1	21	35[c]	74[c]	140[c]	33	100[c]
m/m_0	1	1	0.084	0.090	0.089	0.1	> 0.022

[a]Extracted from Ref. 1.
[b]Nearest-neighbor hopping only at high temperature.
[c]Deduced from the magnetoresistance data.

der the two conditions[22] that (i) the wave function inside the step potential well is not significantly affected by the applied magnetic field (i.e., $\lambda \equiv \sqrt{\hbar c/eH} \gg d$), and (ii) the magnetic potential is smaller than the step potential well (i.e., $d \ll r_{ij} \ll \lambda^2\chi$), the MR in the weak-field limit is then given by Eq. (2) with $p = 2$, $\xi = \chi_{eff}^{-1}$, $t = 0.0015$ for 3D,[36] and $t = 0.0020$ for 2D. Both conditions hold true for our carbon aerogel and ACF samples within the restricted field values of $B < 5$ T and < 73 T, respectively.

Measurements of the temperature dependence of the MR thus serve as a good check for the model in that a consistent set of values for both the effective mass m and the dielectric constant κ, which are shown in Table I, should be obtained from Eqs. (6) and (2).

VII. APPLICATIONS TO GRANULAR AND POROUS SYSTEMS

The application of the CGVRH model to various localization media with different nanostructures is discussed in this section. Each nanostructure studied below corresponds to a limiting case of Eq. (7). For reference, the physical parameters are listed in Table I. The Cermet and the granular aluminum film selected here are the same ones selected in Ref. 6, in which the original CGVRH theory was applied to GM systems.

A. Doped semiconductors

In doped semiconductors, $d \ll s$ (in fact, $d \to 0$). Equation (7) reduces to the situation in doped semiconductors where $\chi_{eff} = \chi_s = 1/\xi$ if ϕ_s is taken to be the ionization potential of a carrier localized in a donor site (i.e., $\hbar^2/2m\xi^2$).

B. Granular metals

Granular metals (GM's) with a low metallic volume fraction (x) and a large experimental T_0 value are usually referred to as Cermets. They differ in structure from the GM systems near the metal-insulator (MI) transition in that in the latter, matrix inversion begins to take place, as corroborated by the observation of a finite empirical value for $\sigma(T = 0)$ in some granular Al films.[37,38] The matrix inversion was also directly observed in the TEM micrographs which show similar morphologies for both the nanopores and the nanoparticles (e.g., see the TEM micrograph for the $x = 0.35$ Au-Al_2O_3 film shown in Ref. 1). The protrusions from the metallic grains into the insulating matrix effectively narrow the gap tunneling distance and allow the image force to lower the gap barrier significantly. The morphology is then similar in both GM's near the MI transition and porous carbons in which $s \ll d$, and suggests the same conduction mechanism for both systems.

A granular aluminum film measured by Chui *et al.*[39] and other GM films[1] near the metal-insulator (MI) transition all have very low values for s and T_0. Using $T_0 = 200$ K from Table I, $\chi_{eff} \simeq \chi_d$, and $\beta = 2.8$, we found that $\kappa \sim 110$ from Eq. (6). Then, $\chi_d^{-1} = 21$ Å, $\chi_d d > 1$, and CGVRH is indeed possible below 30 K, which is about the same temperature at which the experimental $\sigma(T)$ curve begins to deviate from the $p = 2$ law.[39]

On the other hand, in a Ni-SiO_2 Cermet film studied in Ref. 1, in which the $p = 2$ law is followed from 25 K to 300 K, we observe that $\chi_s s \gg \chi_d d$ if κ is taken to be the effective dielectric constant obtained from the effective medium theory (EMT). Then, the N-N hopping should dominate above $T_0/(2\chi_s s)^2 \simeq 30$ K, when the hopping distance $R < 2(s + d)$. In this limit, the distributions in both s and d seem to be adequate for recovering the $p = 2$ law without considering the Coulomb gap,[7–9] which should be exceeded by the hopping energy in the N-N hopping regime. Šimánek[7] derived the following expression for T_0 by solving the bond percolation

problem:

$$k_B T_0 = 0.25 \chi_s s_{\max}^{\rm loc} \epsilon_{\max} , \quad (9)$$

where $s_{\max}^{\rm loc}$ and $\epsilon_{\max}$ are, respectively, the maximum s in the local distribution and the maximum ϵ in the energy distribution. Assuming $s_{\max}^{\rm loc} \sim 2s_{\rm av} = 22$ Å and $\chi_s \simeq 1$ Å^{-1}, we obtained $\epsilon_{\max} \simeq 4e^2/\kappa d \simeq 0.25$ eV, which would give $\kappa \simeq 10$, in good agreement with the κ(EMT) listed in Table I.

In general, the magnetoresistance as a function of both H and T behaves quite differently from one GM to another.[9,38] Because the origin of the magnetoresistance is not limited to the wave-function shrinkage effect studied here, its discussion is beyond the scope of this paper.

C. Activated carbon fibers

In ACF's, the hopping of a charge carrier takes place between two platelets in the in-plane direction because the platelet-to-platelet separation of ~ 10 Å along the c axis, given by the micropore size (see Sec. II), is much larger than that in the in-plane direction. The platelets in the heat-treated ACF's can then be modeled as circular disks aligned in a 2D plane locally as long as the hopping distance is within this local scale. The 2D CGVRH model is therefore used to explain the experimental data for ACF's. The charging energy of each grain also becomes $E_c \sim e^2/\kappa C$, where $C = d/2$ is the capacitance for a circular disk.

When s is as small as a single-bond length, the image-force lowering of ϕ_s (e.g., 11.44 eV Å$/\kappa_{\rm ins} s$, where $\kappa_{\rm ins}$ is the dielectric constant in the insulating gap[40]) could be comparable in magnitude to the work function (~ 4.4 eV in graphite), resulting in $\chi_s s \ll \chi_d d$. Applying Eq. (2) with $t = 0.002$ to the temperature-dependent magnetoresistance data in Fig. 5 for the heat-treated ACF yields $\chi_{\rm eff}^{-1} \simeq 100$ Å. Substituting $\chi_{\rm eff}$ and T_0 extracted from Table I back into Eq. (6) with $\beta = 6.2$ gives $\kappa = 110$, which in turn gives $m_d = 0.022 m_0$, where m_0 is the free-electron mass. We note that a larger and more reasonable value of m_d should be obtained if the divergence of the effective d and κ due to the possible delocalization of carriers over a few grains is considered near the MI transition. For example, when the carrier delocalization is over 5 grains, $m_d \sim 0.1 m_0$, which is a more reasonable value.

For the as-prepared ACF, using the same 2D CGVRH model and assuming a valence-band effective mass of $0.1 m_0$ for the majority hole carriers, we obtain a κ of 58 from Eq. (6) with $\beta = 6.2$. Because there is probably no extended in-plane alignment of the platelets in the as-prepared ACF, as shown in Fig. 2, the 3D CGVRH model might be more appropriate. Using $m_d = 0.1 m_0$, we obtain a more reasonable κ value of 27 for this strongly disordered system.

The large κ values obtained from the CGVRH model reflect the divergence of the dielectric constant of an effective medium near the metal-insulator transition. It is noted that κ is not related to the dielectric constant of the solvent trapped in the micropores, as measured by the capacitance method.

D. Carbon aerogels

As mentioned in Sec. II, carrier hopping takes place between the 12 nm particles in carbon aerogels because of the relative ease of charge transport within one such particle. The view that the transport between nanoparticles cannot be the dominant conduction mechanism is experimentally supported by the strong dependence of both the temperature-dependent conductivity $\sigma(T)$ and the MR on mass density, because only the packing ratio of the particles, and not the internal nanostructure inside the particles, is affected by the mass density.

Constrictions between adjacent grains and an image force again could lower ϕ_s so that $\chi_{\rm eff} \simeq \chi_d$. Following the same procedure used above in the calculation for the heat-treated ACF, and using the average of the two sets of magnetoresistance data in Fig. 8, we estimate that $\chi_{\rm eff}^{-1} \sim 35$, 74, and 140 Å, yielding $\kappa \sim 6$, 31, and 110, and consequently $m_d/m_0 = 0.084$, 0.090, and 0.089 for the $\rho_m = 0.119$ (LD for low density), 0.457 (MD), and 0.645 g/cm^3 (HD) aerogel samples, respectively. The fact that m_d/m_0 varies within a few percent agrees well with the SQUID measurements, which show that the concentration of localized spins within the grains is approximately independent of mass density,[12] thus providing evidence in support for identical nanostructural ordering in samples of all densities. This conclusion is also supported by the photoconductivity measurements.[41] The progressive increase in κ is expected as the aerogel approaches the MI transition. Again, as in the ACF case, the high κ values for the MD and the HD samples are only order-of-magnitude estimates because of the overlap effect near the MI transition. The κ(EMT) values should not be taken literally because EMT is found to be inapplicable to GM systems in general,[9] and near the MI transition, κ should follow some scaling laws.

The onset temperatures (T_c) for CGVRH in Fig. 6 are different for aerogels with different densities. Besides the VRH requirement that $R > 2(s + d)$, namely, that $T_c = 45$, 19, and 10 K for the LD, MD, and HD samples, respectively, we can find a more stringent condition in carbon aerogels specifically, because they consist of crosslinked chains of grains. We define L_n as the average distance within which there is no crosslinking. Then within L_n, only 1D hops are possible and CGVRH only takes place when $R > L_n$. Since the size of the mesopores bounded by the particle chains is approximately inversely proportional to the mass density, L_n should decrease with increasing density. As shown in Fig. 1, which is based on a structural model presented in a previous TEM study,[16] while $L_n \sim 2(s + d)$ in aerogels with higher densities, $L_n \gg 2(s + d)$ for the LD sample, effectively imposing a new condition that $T < T_0/(\chi_d L_n)^2$ for CGVRH in the LD sample. Using $T_c \sim 10$ K and $1/\chi_d = 35$ Å, we can then estimate that in the LD sample $L_n \sim 500$ Å, in agreement with the schematic diagram shown on the left-hand side of Fig. 1, which shows $L_n \sim 4(s+d)$, where

$s+d \simeq 120$ Å is the N-N center-to-center distance. Above T_c, N-N hopping within a chain segment dominates, taking the form of simple thermal activation,[27,42] which is observed in the present work ($p \sim 0.8$ above 10 K). Equation (9) is not followed because there can be no choice in selecting R (an essential ingredient for observing $p \neq 1$ behavior) without a lot of crosslinking.

For the HD sample, the $p = 2$ dependence of $\sigma(T)$ extends up to 300 K, a value higher than T_c. Similarly, a low T_0 value of 190 K was observed up to 300 K in a Au-Al_2O_3 film just below the MI transition with the metallic volume fraction $x = 0.38$. A transition from CGVRH to N-N hopping might have taken place at T_c. As discussed in the conduction mechanism for GM's above, systems below the MI transition exhibited N-N hopping in the form of Eq. (9). The change of the *linear* slopes observed in the $\sigma(T)$ curve for the MD sample in Fig. 6 could be indicative of such a transition. The T_0 values on both sides of the transition are, however, very close, as shown for the HD sample. If we equate $4e^2/\kappa d$ with $\epsilon_{\max}$ when comparing Eq. (9) with Eq. (6), T_0 would be approximately identical in the two equations provided that $\chi_s s_{\max}^{\rm loc}/\chi_d d \simeq 2.6$, which is possible in view of the χ_d and d values listed in Table I, and because of the micropore size of 7 Å, which sets an upper limit for s. In fact, for very small T_0 values, the $1/T^{1/2}$ dependence of $\ln[\sigma(T)]$ is just too weak to permit an accurate evaluation of any change in the T_0 values.

Finally, we comment on the applicability of the fluctuation-induced tunneling (FIT) model, given by[14]

$$\rho(T) = \rho(0) \exp\left(\frac{T_1}{T + T_0}\right) , \qquad (10)$$

where $T_1/T_0 = \pi\chi_s s/2$. Although the three-parameter FIT model fits the data quite well (with values for the fitting parameters given in Table II), the lower limits for the effective mass m/m_0 estimated using $\phi_s = 4.4$ eV and $s \sim 7$ Å are 36, 4.7, and 0.20 for the LD, MD, and HD samples, respectively, two of which are unreasonably large ($\gg 1$) for a conductive solid matrix of graphitic material and probably inconsistent with the SQUID measurements[12] showing the existence of free carriers, which would put E_F above the mobility edge, where the mobility should be large. The widely varied values for m in the three samples also make the FIT model unsatisfactory since both the Raman scattering and the magnetization results imply the same degree of disorder within the carbon particles in each sample, irrespective of the mass density. Our MR results, while supporting the CGVRH model presented in this work, also call into question whether a tunneling mechanism like FIT can give rise to the large MR we observed. Unlike the previous preliminary analysis of our data,[12] we now believe that FIT is not likely in carbon aerogels.

TABLE II. Fitting parameters and effective masses for as-prepared carbon aerogel samples extracted from the fluctuation-induced tunneling model.

Carbon aerogel	~ 0.119 g/cm^3	~ 0.457 g/cm^3	~ 0.645 g/cm^3
T_1 (K) (expt)	71	18	17
T_0 (K) (expt)	1.0	0.7	3.2
m/m_0	36	4.7	0.20

VIII. CONCLUSIONS

With energy fluctuations among the grains, variable-range hopping (VRH) becomes a possibility. A Coulomb gap model is introduced to explain the $\sigma(T) = \sigma_0 \exp[-(T_0/T)^{1/2}]$ behavior observed experimentally at low temperature. It is found that this model might be applicable to granular metallic systems previously studied near the metal-insulator transition. The model is also consistent with both the conductivity and the magnetoresistance results for carbon aerogels and activated carbon fibers, which are porous materials with a necessarily uneven spatial distribution of grains, thus constituting a complementary class of granular metallic systems for studying granularity and its effect on localization phenomena. The transport measurements are sensitive to the nanostructure of carbon aerogels and should provide new characterization tools for the design of aerogel materials in general.

ACKNOWLEDGMENTS

We are grateful to Dr. K. Kuriyama of the Sumitomo Metal Industries Ltd., Japan, for kindly supplying the heat-treated activated carbon fiber samples. The MIT authors gratefully acknowledge the Lawrence Livermore National Laboratory for support of this research under Subcontract No. B130530. The aerogel synthesis was performed under the auspices of the U.S. Department of Energy by Lawrence Livermore National Laboratory under Contract No. W-7405-ENG-48.

[1] B. Abeles, P. Sheng, M. D. Coutts, and Y. Arie, Adv. Phys. **24**, 407 (1975).
[2] A. W. P. Fung, J. J. Chen, Z. H. Wang, M. S. Dresselhaus, and R. W. Pekala, in *Extended Abstracts of the 21st Biennial Conference on Carbon, Buffalo, NY, 1993*, edited by D. D. L. Chung (Am. Carbon Soc., University Park, PA, 1993), p. 659.
[3] A. W. P. Fung, A. M. Rao, K. Kuriyama, M. S. Dresselhaus, G. Dresselhaus, and M. Endo, J. Mater. Res. **8**, 489 (1993).
[4] A. W. P. Fung, M. S. Dresselhaus, and M. Endo, Phys. Rev. B **48**, 14 953 (1993).
[5] C. J. Adkins, J. Phys. C **20**, 235 (1987).
[6] C. J. Adkins, in *Hopping and Related Phenomena*, edited by H. Fritzsche and M. Pollak (World Scientific, Singapore, 1990), p. 93.
[7] E. Šimánek, Solid State Commun. **40**, 1021 (1981).
[8] P. Sheng and J. Klafter, Phys. Rev. B **27**, 2583 (1983).

[9] P. Sheng, Philos. Mag. B **65**, 357 (1992).
[10] E. B. Foxman, P. L. McEuen, U. Meirav, N. S. Wingreen, Y. Meir, P. A. Belk, N. R. Belk, and M. A. Kastner, Phys. Rev. B **47**, 10 020 (1992).
[11] M. P. J. van Staveren, H. B. Brom, and L. J. de Jongh, Phys. Rep. **208**, 1 (1991).
[12] A. W. P. Fung, Z. H. Wang, K. Lu, M. S. Dresselhaus, and R. W. Pekala, J. Mater. Res. **8**, 1875 (1993), and references therein.
[13] A. L. Efros and B. I. Shklovskii, J. Phys. C **8**, L49 (1975).
[14] P. Sheng, E. K. Sichel, and J. J. Gittleman, Phys. Rev. Lett. **40**, 1197 (1978).
[15] R. W. Pekala and C. T. Alviso, in *Novel Forms of Carbon*, edited by C. L. Renschler, J. J. Pouch, and D. M. Cox, MRS Symposia Proceedings No. 270 (Materials Research Society, Pittsburgh, 1992), p. 3.
[16] G. C. Ruben, R. W. Pekala, T. M. Tillotson, and L. W. Hrubesh, J. Mater. Sci. **27**, 4341 (1992).
[17] A. M. Rao, A. W. P. Fung, M. S. Dresselhaus, G. Dresselhaus, and M. Endo, in *Extended Abstracts of the 20th Biennial Conference on Carbon, Santa Barbara, CA, 1991*, edited by R. A. Meyer (Am. Carbon Soc., University Park, PA, 1991), p. 242.
[18] A. M. Rao, A. W. P. Fung, M. S. Dresselhaus, and M. Endo, J. Mater. Res. **7**, 1788 (1992).
[19] E. Tanaka, Fuel Combust. **54**, 241 (1987).
[20] A. W. P. Fung, A. M. Rao, K. Kuriyama, M. S. Dresselhaus, and G. Dresselhaus, in *Defects in Materials*, edited by P. D. Bristowe, J. E. Epperson, J. E. Griffith, and Z. Liliental-Weber, MRS Symposia Proceedings No. 209 (Materials Research Society, Pittsburgh, 1991), p. 335.
[21] K. Kuriyama and M. S. Dresselhaus, J. Mater. Res. **7**, 940 (1992).
[22] B. I. Shklovskii and A. L. Efros, *Electronic Properties of Doped Semiconductors*, Springer Series in Solid-State Sciences, Vol. 45 (Springer, Berlin, 1984).
[23] J. Heinrichs, A. A. Kumar, and N. Kumar, J. Phys. C **9**, 3249 (1976).
[24] K. D. Leaver, J. Phys. C **10**, 249 (1977).
[25] K. Kuriyama and M. S. Dresselhaus, J. Mater. Res. **6**, 1040 (1991).
[26] G. A. M. Reynolds, Z. H. Wang, M. S. Dresselhaus, A. W. P. Fung, and R. W. Pekala, Phys. Rev. B **49**, 15 027 (1994).
[27] W. Brenig, G. H. Döhler, and H. Heyszenau, Philos. Mag. **27**, 1093 (1973).
[28] A. Miller and E. Abrahams, Phys. Rev. **120**, 745 (1960).
[29] O. Entin-Wohlman, Y. Gefen, and Y. Shapira, J. Phys. C **16**, 1161 (1983).
[30] R. Kubo, J. Phys. Soc. Jpn. **17**, 975 (1962).
[31] W. P. Halperin, Rev. Mod. Phys. **58**, 533 (1986).
[32] A. L. Efros, N. Van Lien, and B. I. Shklovskii, Solid State Commun. **32**, 851 (1979).
[33] A. L. Efros, J. Phys. C **9**, 2021 (1976).
[34] S. D. Baranovskii, A. L. Efros, B. L. Gelmont, and B. I. Shklovskii, Solid State Commun. **27**, 1 (1978).
[35] H. Scher and R. Zallen, J. Chem. Phys. **53**, 3759 (1970).
[36] I. S. Shlimak, A. N. Ionov, and B. I. Shklovskii, Fiz. Tekh. Poluprovodn. **17**, 503 (1983) [Sov. Phys. Semicond. **17**, 314 (1983)].
[37] W. L. McLean, P. Lindenfeld, and T. Worthington, in *Electrical Transport and Optical Properties of Inhomogeneous Media*, edited by J. C. Garland and D. B. Tanner, AIP Conf. Proc. No. 40 (AIP, New York, 1978), p. 403.
[38] W. L. McLean, T. Chui, B. Bandyopadhyay, and P. Lindenfeld, in *Inhomogeneous Superconductors*, Proceedings of the International Conference on Inhomogeneous Superconductors, Berkeley Springs, WV, 1979, edited by D. U. Gubser, T. L. Francavilla, S. A. Wolf, and J. R. Leibowitz, AIP Conf. Proc. No. 58 (AIP, New York, 1980), p. 42.
[39] T. Chui, G. Deutscher, P. Lindenfeld, and W. L. McLean, Phys. Rev. B **23**, 6172 (1980).
[40] J. G. Simmons, in *Tunneling Phenomena in Solids*, edited by E. Burstein and S. Lundqvist (Plenum Press, New York, 1969), p. 135.
[41] M. Hosoya, G. Reynolds, and M. S. Dresselhaus, J. Mater. Res. **8**, 811 (1993).
[42] J. Kurkijärvi, Phys. Rev. B **8**, 922 (1973).
[43] M. Smíšek and S. Černý, *Active Carbon: Manufacture, Properties and Applications* (Elsevier, New York, 1967).